IET Power Electronics

Research Article

IET Journals
The Institution of Engineering and Technology

Multiport bidirectional DC–DC converter for PV powered electric vehicle equipped with battery and supercapacitor

ISSN 1755-4535
Received on 21st June 2020
Revised 20th November 2020
Accepted on 23rd November 2020
E-First on 19th January 2021
doi: 10.1049/iet-pel.2020.0759
www.ietdl.org

Murat Mustafa Savrun[1] ✉, *Alihan Atay*[2]

[1]*Department of Electrical & Electronics Engineering, Adana Alparslan Türkeş Science and Technology University, Adana, Turkey*
[2]*Solvaytech Engineering Industry and Trade Ltd Co., Adana, Turkey*
✉ *E-mail: msavrun@atu.edu.tr*

Abstract: This study presents a novel quasi-Z-source converter integrated isolated multiport bidirectional DC–DC converter topology for a photovoltaic (PV) powered and battery/supercapacitor buffered electric vehicle (EV). The proposed topology can provide uninterrupted power to the electric motor of EV and regain the braking energy with the capability of bidirectional power flow. The system integrates quasi-Z-source and H-bridge converters with an existing switch. Thus, a four-port converter is achieved without any need for individual converters or additional switches. Besides, the high-gain quasi-Z-source converter allows the reduction of the rated voltages of the battery and supercapacitor packs, as well as allows using a high-frequency transformer (HFT) with a low turn ratio. The isolation between ports is provided by a secondary centre-tapped HFT. The secondary side of the HFT is equipped with a controlled full-wave rectifier to provide bidirectional power flow. In addition, a power flow management and corresponding control scheme are suggested. The performance of the proposed system has been evaluated for different operational changes. Results show that it properly performs the power flow between the ports under steady-state and transient conditions. The power flow capabilities and efficiency values validate the viability and effectiveness of the proposed system.

1 Introduction

Nowadays, the interest in renewable energy sources (RESs) such as photovoltaic (PV) or fuel cell is increasing in parallel with the rapidly depleting fossil fuels and increasing greenhouse gas emissions. Therefore, power systems equipped with RESs are frequently preferred. Owing to the intermittent nature of RESs, energy storage units (ESUs) play a key role to provide uninterrupted power to the loads in these types of power systems. Besides, the power electronic converters are the other essential components to supervise the power flow between the RESs, storage units, and loads. Fig. 1 shows the conventional RES-based power system equipped with an ESU. The power produced by the RES is transferred directly to the loads or storage units, while the batteries are charged or discharged depending on the instantaneous production values of RESs and demands of loads. Power transfers between the units are carried out through independent power electronics converters are the main interface element.

Recently, several studies have been performed regarding the integrated power electronic converters used in a system with multiple RESs or storage units (i.e. hybrid energy systems). Especially, multiport DC–DC converters or the reduced switch form of them are employed because of the compact structures with reduced complexity, a lower cost, and fewer component counts [1–4]. The multiport converters (MPCs) are categorised into two as isolated and non-isolated converters and are presented in [5–7]. Non-isolated MPCs had been derived from the buck, boost, buck–boost converter topologies with features of compact design and high-power density. The non-isolated forms of MPCs developed in [8–11] are used to meet the requirements of an EV equipped with a battery/ultracapacitor, such as high energy/power density, and long battery life.

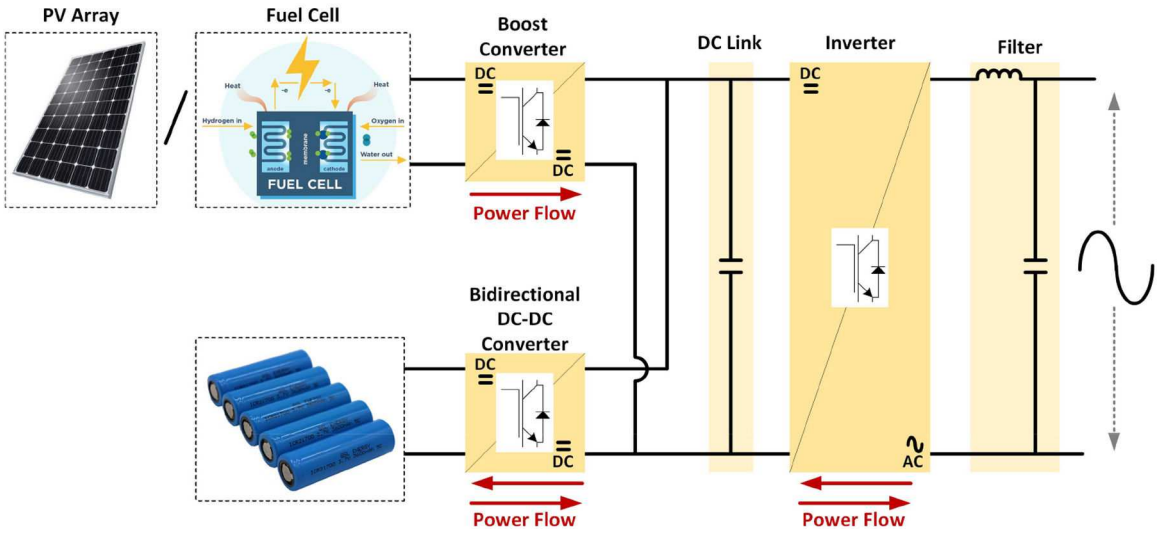

Fig. 1 *Conventional RES-based power system*

Isolated MPCs are usually composed of variations of the bridge topologies for critical applications that require isolation. Many studies have addressed isolated converters considering large conversion ratios and isolation requirements [12]. The common aspect of isolated topologies is the use of high-frequency transformers (HFTs). Although the HFT increases the complexity of the system, it provides flexibility with a high conversion ratio in voltage level and also isolates the ports. The isolated topologies can be classified by considering the rest of the topology. Studies that used the topology of the dual active bridge (DAB) converter are frequently encountered in the literature [13]. The related topology makes it possible to use zero voltage switching and phase shift operations to improve the performance of the system [14, 15]. As a variant of the DAB topology, MPC topologies are derived using multi-winding HFTs. In [14, 16–18], full-bridge converter-based MPCs are realised by employing multi-winding HFTs. The related topology provides both galvanic isolation and bidirectional power transfer between all ports. Besides, full-bridge converter-based MPCs equipped with resonant tanks have been developed to improve the efficiency of the overall converters [19]. Some studies focus on the MPC topologies equipped with a half-bridge converter with the disadvantages of a narrow duty cycle rather than the full-bridge converter [20]. The main drawbacks of the MPC topologies endowed with multi-winding HFTs and their variations are that many switching devices are used and the control complexities are high.

In the reduced switch topology context, some authors have addressed interleaved MPC topologies interfacing input/output ports using two-winding HFTs [21, 22]. The related topologies have been designated as partially isolated because they provide isolation between the primary and secondary sides of the HFT rather than all ports [23]. The topology proposed in [21] consists of three ports through the primary side interleaved structure whereas, in [22], four ports are integrated through the dual interleaved structure. Besides, various interleaved topologies are suggested in [21, 24]. In the proposed interleaved topologies, a maximum of two input ports is employed. In addition to these topologies, a partially isolated full-bridge based MPC integrated with a bidirectional buck/boost converter is suggested in [25]. Although the proposed topology enables the battery to be charged by the PV, it cannot perform bidirectional power transfer because of the diode rectifier integrated to the secondary side of the HFT. In addition, topologies equipped with centre-tapped HFTs have been discussed in [6, 26–30]. In [29, 30], topologies accompanied by a primary side equipped with an H-bridge driven in a phase-shifting manner and a secondary side equipped with a centre tap type rectifier have been proposed. These topologies have the advantages of a wide zero-voltage-switching range, no problems related to duty-cycle loss, no circulating current, and the reduction of secondary-voltage oscillation and overshoot. Although topologies in [29, 30] differ from each other in that the rectifier configurations of the secondary side and the design of controllers are slightly different, both topologies have one-input and one-output ports.

As it is understood from the literature review, the partially isolated topologies offer a compact design and low cost when compared with the fully isolated topologies. However, the suggested topologies provide constrained voltage gain through the HFTs turns ratio and need more switches to increase the number of ports.

This paper proposes a novel isolated multiport bidirectional DC–DC converter topology integrated with a quasi-Z-source converter (qZ_iMPC) for a PV powered electric vehicle (EV) equipped with battery and supercapacitor. Besides, a power flow management and a corresponding control scheme are suggested. The proposed converter is composed of a secondary centre-tapped HFT, an H-bridge converter, a controlled full-wave rectifier, and a quasi-Z-source converter. The qZ_iMPC makes it possible to achieve a high-voltage gain with low-input battery/supercapacitor voltage and less duty cycle through the quasi-Z-source converter. Compared with the converters presented in the literature, the proposed converter uses less number of active switches to integrate four ports and allows bidirectional power flow. The performance of the proposed system is verified with different case studies.

The rest of the paper is organised as follows: Section 2 introduces the proposed multiport converter topology and describes its operation principle. Section 3 presents the design of the control algorithm for the proposed multiport converter. The results of case studies are presented in Section 4. Section 5 puts forward conclusions with relevant discussion.

2 Proposed converter and operation principle

2.1 Proposed qZ_iMPC topology

In this paper, a novel four-port converter topology is proposed. The proposed qZ_iMPC topology is illustrated in Fig. 2, which consists of a secondary centre-tapped HFT, an H-bridge converter, a controlled full-wave rectifier, and a quasi-Z-source converter. The electric motor (EM) of the EV, which is assumed as a load, is fed by a PV system and buffered by an ESU to provide constant voltage (CV) to the motor drive of the EV. The ESU is composed of a battery pack to supply the EM under steady-state conditions, and a supercapacitor pack to suppress the impact of the inrush current during transients to avoid the adverse effect on the battery pack. The qZ_iMPC makes it possible to achieve high-voltage gain using a quasi-Z-source converter on the ESU side. Thus, the number of series supercapacitors decreases in parallel with the low amount of supercapacitor pack voltage and less duty cycle ability. The secondary side of the HFT is equipped with a controlled full-wave rectifier. The freewheeling diodes of the switches are biased and act as a full-wave rectifier for the power flow towards the EM, while active switches are triggered for the power flow towards the ESU.

As shown in Fig. 2, the phase-shifted full-bridge DC–DC converter shares S_2 switch with the quasi-Z-source DC–DC converter. Hereby, quasi-Z-source and full-bridge converters are integrated at the primary side of the HFT. The battery pack and supercapacitor pack are able to charge via the PV when the production capacity of PV is higher than the EM demand, or via the EM during regenerative braking is active. The ESU provides the power demand of the EM in the case of insufficient irradiation across the PV. A power flow management system monitors the instantaneous power generation of PV and varying EM demands. Thus, the power flow is performed between the PV, ESU, and EM in various cases. Besides, the converter is controlled with perturb and observe (P&O) maximum power point tracking (MPPT), DC-link control, and constant current (CC)/CV charging algorithms.

2.2 Operation principle of the proposed converter

The proposed topology has three different working modes according to the instantaneous power values of PV and EM; when the energy is transferred from PV to EM and ESU, the converter operates in mode 1; when energy is transferred from PV and ESU to EM, the converter operates in mode 2; when energy is transferred from EM to ESU, the converter operates in mode 3. The operation stages and current flows during the modes are presented in detail in Figs. 3–6. Fig. 3*a* shows the switching sequence diagram when the converter operates in mode 1, where T_s is the switching cycle of S_1–S_6. As shown in Fig. 3*a*, the converter has four operation stages during one switching cycle when operating in mode 1. The value of D determines both the gain of the quasi-Z-source converter and the direction of power flow. D varies within the interval of 0–0.5. S_5 and S_6 switches are off position; however, freewheeling diodes of these two switches act as a full-wave rectifier. Fig. 4 shows the current flow in mode 1.

Stage 1 [t_1–t_2]: At t_1, S_1 switch is turned ON. As a quasi-Z-source circuit operates in a non-shoot through the state, i_{Lq1} and i_{Lq2} currents increase gradually until the time point t_2. Also, the battery pack and supercapacitor pack are charged through the PV. On the other hand, the S_4 switch is turned ON until the time point t_2. In this manner, the primary voltage of HFT is equal to PV voltage. The current of PV is equal to the sum of the HFT primary current and ESU current. Meanwhile, the freewheeling diode of the S_5 switch is turned ON and PV power is transferred to the EM.

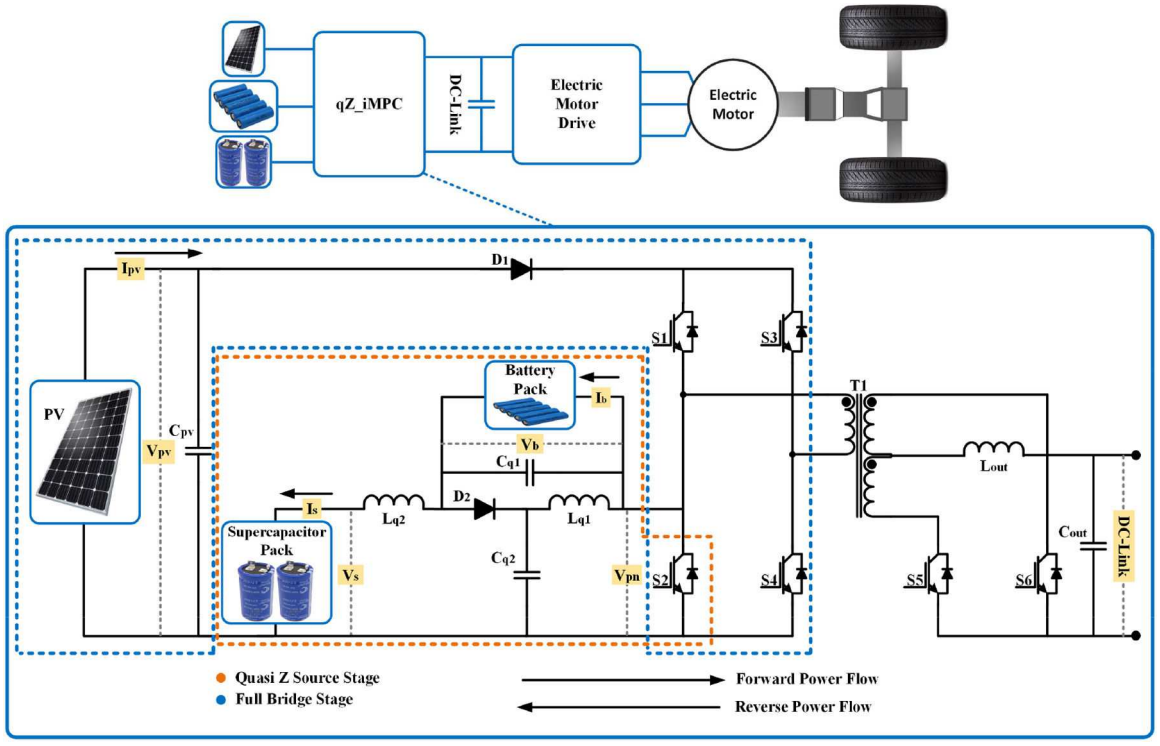

Fig. 2 *Novel quasi-Z-source integrated isolated multiport DC–DC converter*

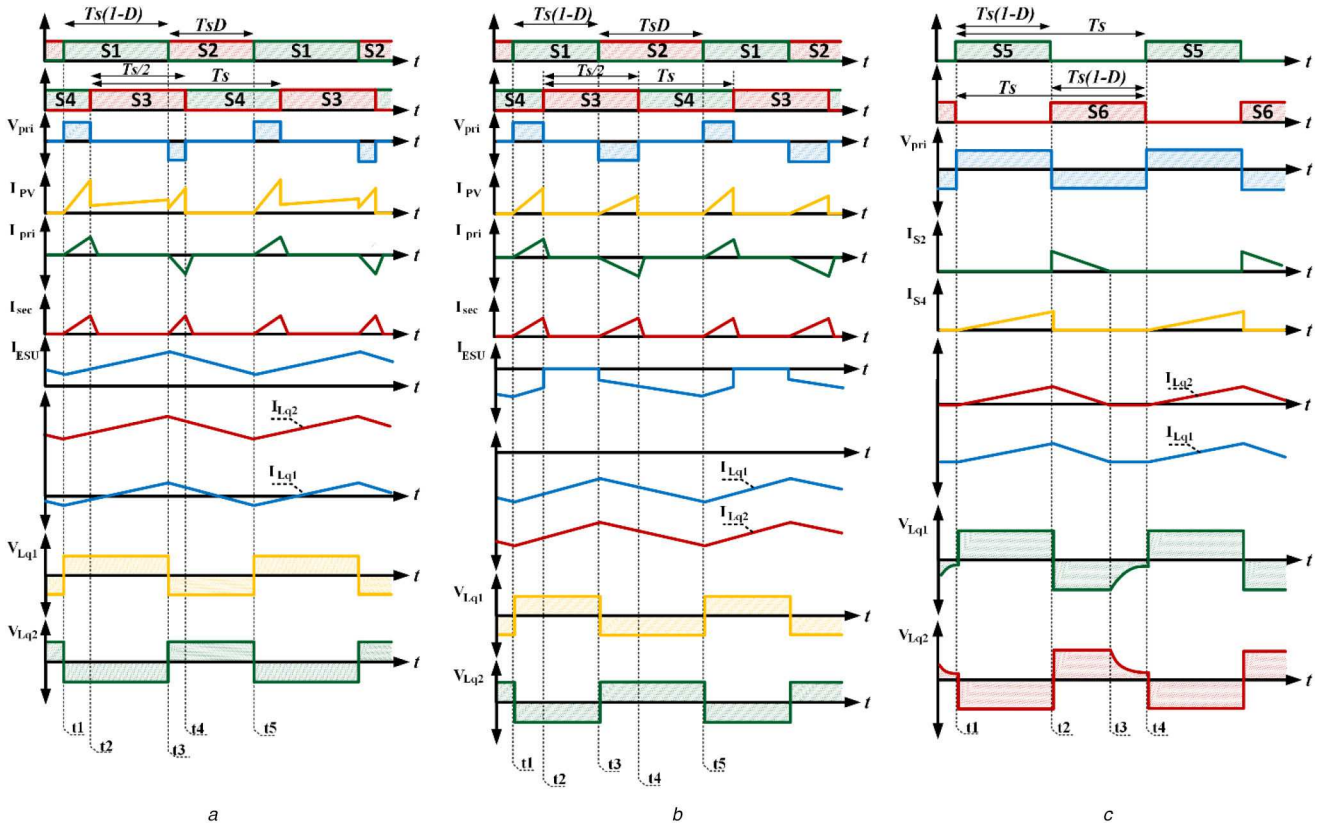

Fig. 3 *Switching sequence diagrams of*
(a) Mode 1, ***(b)*** Mode 2, ***(c)*** Mode 3

Stage 2 [t_2–t_3]: At t_2, S_3 switch is turned ON. As a quasi-Z-source circuit still operates in a non-shoot through the state, i_{Lq1} and i_{Lq2} currents increase gradually until the time point t_3. Also, the battery pack and supercapacitor pack are charged through the PV. However, power transfer from PV to EM is completed because S_1 and S_3 switches are turned ON at this stage. The PV current is equal to the ESU current and also primary and secondary currents of HFT decrease to zero. Meanwhile, a freewheeling diode of the S_5 switch is turned ON and the energy of the HFT is transferred to the EM. When the primary and secondary currents of the HFT reach zero, the freewheeling diode of the S_6 switch is turned ON and EM is fed from the output capacitor (C_{out}).

Stage 3 [t_3–t_4]: At t_3, the S_2 switch is turned ON. As a quasi-Z-source circuit operates in a shoot-through state, and battery pack and supercapacitor pack are not charged through the PV, i_{Lq1} and i_{Lq2} currents decrease gradually until the time point t_4. On the other

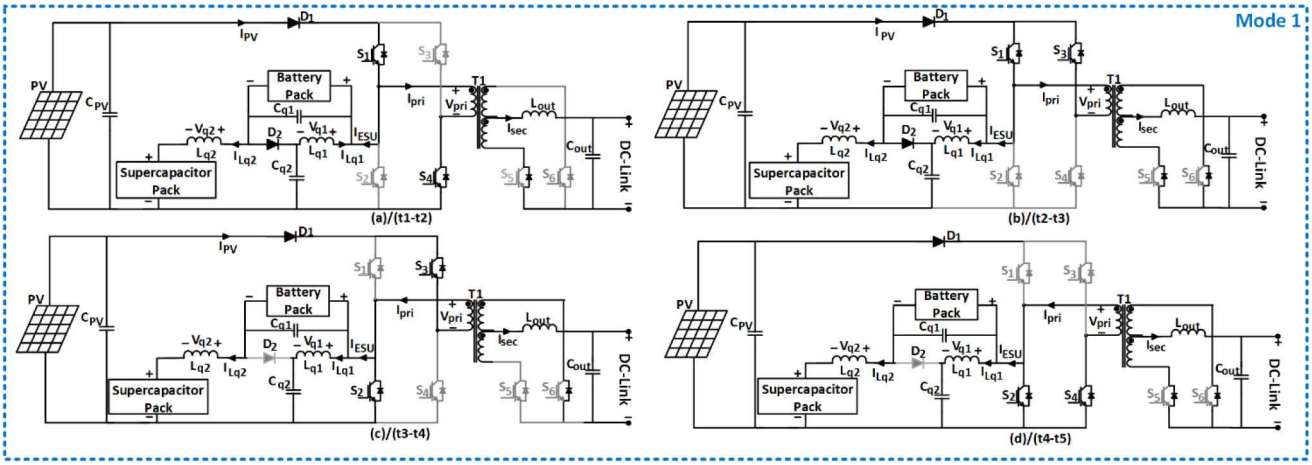

Fig. 4 *Current flow paths of mode 1*
(a) Stage 1 (t_1–t_2), ***(b)*** Stage 2 (t_2–t_3), ***(c)*** Stage 3 (t_3–t_4), ***(d)*** Stage 4 (t_4–t_5)

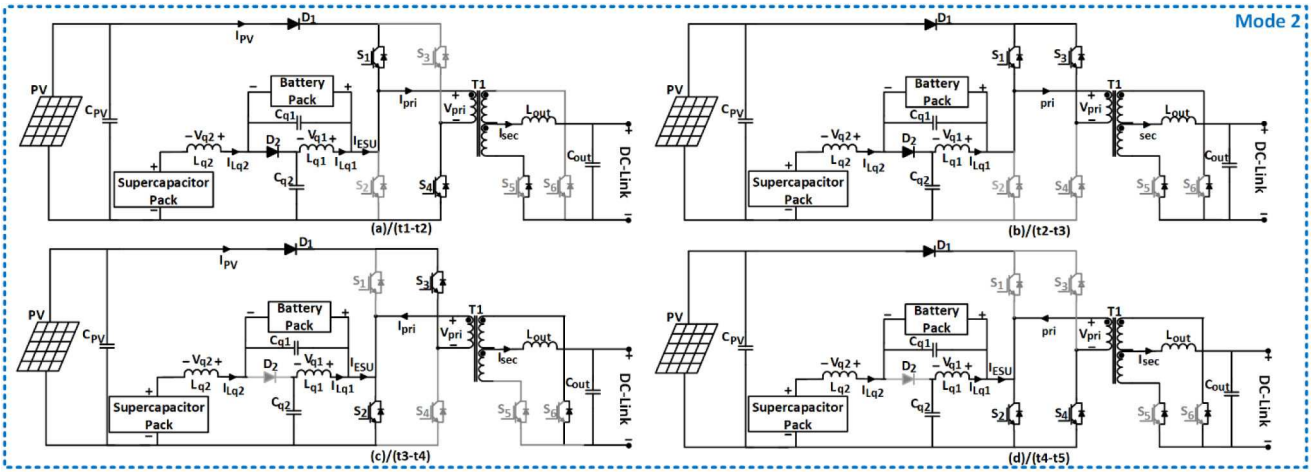

Fig. 5 *Current flow paths of mode 2*
(a) Stage 1 (t_1–t_2), ***(b)*** Stage 2 (t_2–t_3), ***(c)*** Stage 3 (t_3–t_4), ***(d)*** Stage 4 (t_4–t_5)

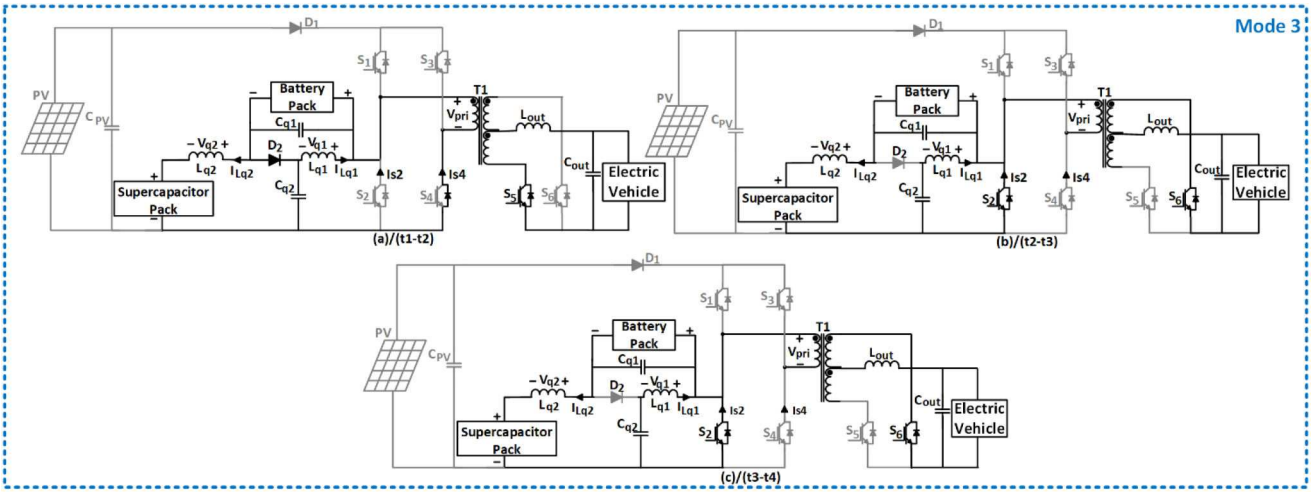

Fig. 6 *Current flow paths of mode 3*
(a) Stage 1 (t_1–t_2), ***(b)*** Stage 2 (t_2–t_3), ***(c)*** Stage 3 (t_3–t_4)

hand, the S_3 switch is turned ON at this stage. In this manner, the primary voltage of HFT is equal to the negative PV voltage, and also the primary current of HFT is equal to the negative PV current. However, the ESU current is not equal to zero and decreases gradually until the time point t_4. Meanwhile, the freewheeling diode of the S_6 switch is turned ON and PV power is transferred to the EM.

Stage 4 [t_4–t_5]: At t_4, the S_4 switch is turned ON. As a quasi-Z-source circuit still operates in a shoot-through state, i_{Lq1} and i_{Lq2} currents decrease gradually until the time point t_5. Also, the battery pack and supercapacitor pack are not charged through the PV. However, power transfer from PV to EM is finished because S_2 and S_4 switches are ON at this stage. Therefore, the PV current is equal to zero at time point t_4, and also the primary and secondary currents of HFT reach zero. The ESU current decreases gradually until the

time point t_5. Meanwhile, the freewheeling diode of the S_6 switch is turned ON and the energy of the HFT is transferred to the EM. When the primary and secondary currents of the HFT reach zero, the freewheeling diode of the S_5 switch is turned ON and the EM is fed from the output capacitor (C_{out}).

The switching sequence diagram when the converter operates in mode 2 is illustrated in Fig. 3*b*. The converter has four operation stages during one switching cycle when operating in mode 2. D varies within the interval of 0.5–1. S_5 and S_6 switches are turned OFF, however, freewheeling diodes of these two switches act as a full-wave rectifier. Fig. 5 shows the current flow in mode 2.

Stage 1 [t_1–t_2]: At t_1, S_1 switch is turned ON. As a quasi-Z-source circuit operates in a non-shoot-through state, i_{Lq1} and i_{Lq2} currents increase gradually until the time point t_2. Also, the battery pack and supercapacitor pack are discharged. On the other hand, the S_4 switch is ON until the time point t_2. In this manner, the primary voltage of HFT is equal to PV voltage. The HFT primary current is equal to the sum of the PV current and the ESU current. Meanwhile, the freewheeling diode of the S_5 switch is turned ON and PV and ESU power is transferred to the EM.

Stage 2 [t_2–t_3]: At t_2, S_3 switch is turned ON. As a quasi-Z-source circuit still operates in a non-shoot-through state, i_{Lq1} and i_{Lq2} currents increase gradually until the time point t_3. Power transfer from PV to EM is finished because S_1 and S_3 switches are turned ON at this stage. The currents of PV and ESU are equal to zero at time point t_2 and the primary and secondary currents of HFT decrease to zero. Meanwhile, the freewheeling diode of the S_5 switch is turned ON and the energy of the HFT is transferred to the EM. When the primary and secondary currents of the HFT reach zero, the freewheeling diode of the S_6 switch is turned ON and the EM is fed from the output capacitor (C_{out}).

Stage 3 [t_3–t_4]: At t_3, the S_2 switch is turned ON. As a quasi-Z-source circuit operates in a shoot-through state, i_{Lq1} and i_{Lq2} currents decrease gradually until the time point t_4. On the other hand, the S_3 switch is turned ON at this stage. In this manner, the primary voltage of HFT is equal to the negative PV voltage. Also, the primary current of HFT is equal to the negative PV current. However, the ESU current decreases gradually until the time point t_4. Meanwhile, the freewheeling diode of the S_6 switch is turned ON and PV power is transferred to the EM.

Stage 4 [t_4–t_5]: At t_4, the S_4 switch is turned ON. As a quasi-Z-source circuit still operates in a shoot-through state, i_{Lq1} and i_{Lq2} currents decrease gradually until the time point t_5. Power transfer from the PV to the EM is complete because S_2 and S_4 switches are turned ON at this stage. Therefore, the PV current is equal to zero at time point t_5, and also the primary and secondary currents of HFT are decreased. The ESU current decreases gradually until the time point t_5. Meanwhile, the freewheeling diode of the S_6 switch is turned ON and the energy of the HFT is transferred to the EM. When the primary and secondary currents of the HFT reach zero, the freewheeling diode of the S_5 switch is turned ON and the EM is fed from the output capacitor (C_{out}).

The switching sequence diagram when the converter operates in mode 3 is illustrated in Fig. 3*c*. The converter has three operation stages during one switching cycle. D varies within the interval of 0–1. D_1 diode is reverse biased; therefore, no current flows towards the PV. Fig. 6 shows the current flow in mode 3.

Stage 1 [t_1–t_2]: At t_1, the S_5 switch is turned ON. At this time, the primary voltage of the HFT is equal to the DC-link voltage. Therefore, the freewheeling diode of the S_4 switch is turned ON and the freewheeling diode of the S_2 switch is turned OFF. Meanwhile, the quasi-Z-source circuit operates in a non-shoot-through state, i_{Lq1} and i_{Lq2} currents increase gradually until the time point t_2.

Stage 2 [t_2–t_3]: At t_2, the S_6 switch is turned ON. At this time, the primary voltage of the HFT is equal to the negative DC-Link. Therefore, the freewheeling diode of the S_2 switch is turned ON and the freewheeling diode of the S_4 switch is turned OFF. Meanwhile, the quasi-Z-source circuit operates in a shoot-through state, i_{Lq1} and i_{Lq2} currents decrease gradually until the time point t_3.

Stage 3 [t_3–t_4]: In this time interval, the primary voltage of the HFT is equal to the negative DC-link; however, the S_2 switch current flow reaches zero. Also, i_{Lq1} and i_{Lq2} are constant during this stage. Therefore, v_{Lq1} and v_{Lq2} voltages decrease gradually until the time point t_4.

Considering the operation modes of the ESU, the relationship between the PV voltage (V_{PV}) and battery voltage (V_b) is computed using the S_2 duty cycle (D) [25]. It is expressed as follows:

$$V_{PV} = \frac{V_b}{D} \tag{1}$$

During the time interval of non-shoot-through and shoot-through states, inductor voltages and currents of the quasi-Z-source converter are computed according to (2) and (3), respectively [31]

$$V_{Lq2} = V_s - V_{Cq2},\ V_{Lq1} = -V_{Cq1},\ V_{pn} = V_{Cq2} - V_{Lq1} = V_{Cq1} + V_{Cq2},\ V_{D2} = 0 \tag{2}$$

$$V_{Lq2} = V_s + V_{Cq1},\ V_{Lq1} = V_{Cq2},\ V_{pn} = 0,\ V_{D2} = (V_{Cq1} + V_{Cq2}) \tag{3}$$

where V_s and V_{pn} represent the supercapacitor voltage and output voltage of the quasi-Z-source converter, respectively.

At the steady-state, the average voltages of the inductors are zero for one switching cycle. Thus, the voltages of the capacitors can be derived as follows:

$$V_{Lq1} = \frac{DT_s(V_{Cq2}) + (1-D)T_s(-V_{Cq1})}{T_s} = 0 \tag{4}$$

$$V_{Lq2} = \frac{DT_s(V_{Cq1} + V_s) + (1-D)T_s(V_s - V_{Cq2})}{T_s} = 0 \tag{5}$$

$$V_{Cq1} = \frac{D}{1-2D}V_S \tag{6}$$

$$V_{Cq2} = \frac{1-D}{1-2D}V_S \tag{7}$$

At the steady-state, the relationship between battery voltage and supercapacitor voltage is defined as follows [32]:

$$V_{pn} = V_{Cq1} + V_{Cq2} = \frac{1}{1-2D}V_S \tag{8}$$

3 Proposed multi-loop control scheme

The controller of the proposed multiport system performs to meet multi-control objectives such as power flow management, MPPT, CC/CV charging, and DC-link control. The optimal power flow between the PV, ESU, and EM is achieved with the ability of the power allocation of the controller. The main aims of power flow management are: (i) to provide the supplying continuity of the EM considering the limits of the PV and ESU and (ii) to provide reverse power flow to regain the braking energy. The control of the overall system is performed by the overall controller structure shown in Fig. 7.

The power flow management strategy assigns modes of operation of the system considering the available PV power, EM demand, and ESU state such as

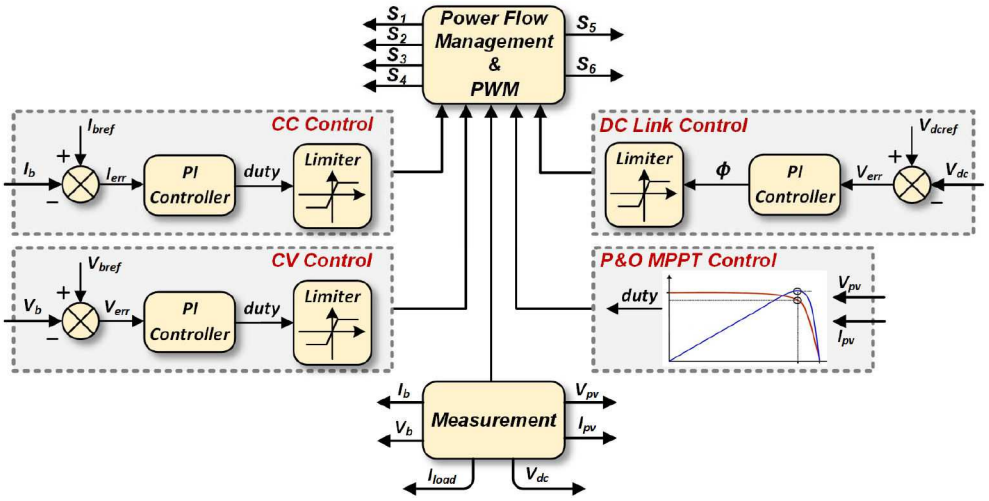

Fig. 7 *Overall control structure of the proposed system*

```
begin
number v, v_old, i, p, p_old, ref, ref_old, ref_delta
input v,i
p = v*i
if ((p – p_old) != 0) then
      if ((p – p_old)  <  0) then
            if (v – v_old < 0) then
                  ref = ref_old – ref_delta
            else
                  ref = ref_old + ref_delta
            endif
      else
            if (v – v_old < 0) then
                  ref = ref_old + ref_delta
            else
                  ref = ref_old – ref_delta
            endif
      endif
else
      ref = ref_old
endif
ref_old = ref
v_old = v
p_old = p
output ref
end
```

Fig. 8 *P&O pseudo-code*

Mode 1: This mode corresponds to a PV power (P_{PV}) greater than the power demanded by the EM (P_{Em}). In this state, there is a surplus of energy to be stored in the ESU (P_{ESU}). PV charges the battery and the supercapacitor while feeding the EM with the reference powers are given by the following equations:

$$\begin{aligned} P_{PV} &> P_{EM} \\ P_{ESU} &= P_{PV} - P_{EM} \end{aligned} \tag{9}$$

Mode 2: This mode corresponds to a PV power less than the power demanded by the EM. In this state, there is a lack of energy that should be buffered by the ESU. Therefore, the EM is fed by both PV and ESU. The reference powers are given by the following equations:

$$\begin{aligned} P_{PV} &< P_{EM} \\ P_{EM} &= P_{PV} + P_{ESU} \end{aligned} \tag{10}$$

Mode 3: This mode corresponds to a braking power that occurs during the braking of an EV with regenerative capability. In this state, there is an energy that is transformed into electrical energy from kinetic energy and is stored in the ESU. So, the battery and supercapacitor are charged by the EM. The reference powers are given by the following equations:

$$\begin{aligned} P_{PV} &= 0 \\ P_{ESU} &= P_{EM} \end{aligned} \tag{11}$$

According to the different power values of PV and EM, qZ-iMPC is controlled to work in different modes. By distributing the control domain properly, an automatic transition between these modes can be realised. Fig. 7 shows the control diagram for the proposed converter. There are four control loops as follows: P&O MPPT control loop, DC-link control loop, CC control loop, and CV control loop. A modified phase-shift modulation scheme is adopted to control the full-bridge under forward power flow conditions. The switches S_3 and S_4 have a constant duty cycle (50%) with a 180° phase shift between each other, whereas the duty cycles of complementary switches S_1 and S_2 vary considering the state determined by the power flow management system. While the phase shift between S_1 and S_4/S_2 and S_3 provides DC-link control, the duty cycle of the switches S_1 and S_2 provides maximum power transfer by controlling the output voltage of PV or provides bidirectional power flow for the ESU.

The maximum power transfer is performed by the P&O MPPT method due to the ease of operation and reduced computational load. The controller monitors the output voltage and current of PV and computes the instantaneous available power. The algorithm perturbs the operating voltage to ensure maximum power. The operational algorithm of the P&O method is explained by a pseudo-code in Fig. 8.

The excessive power of the PV is transferred to the ESU using the CC–CV charging algorithms during mode 1 according to (6). The controller prevents the charging current from exceeding half of the battery pack capacity (i.e. 0.5 C). When the charge current of the battery pack reaches the reference value of 30 A (I_{bref}), the controller keeps the charge current constant. The CC control continues until the battery voltage rises to the reference value of 217.8 V (V_{bref}). The CC charging is followed by the CV charging, and the charge current gradually decreases to 0.05 C and the charging process completes. The CC–CV charging is achieved by regulating the duty cycles of the switches S_1 and S_2. Besides, CC–CV charging is performed by adjusting the duty cycles of S_5 and S_6 switches during mode 3. The difference between the measured current (I_b)/voltage (V_b) and the determined reference current (I_{bref})/voltage (V_{bref}) for each control is obtained and applied to the proportional–integral (PI) controllers for CC and CV charging algorithms, respectively. The ESU and PV feed the EM during

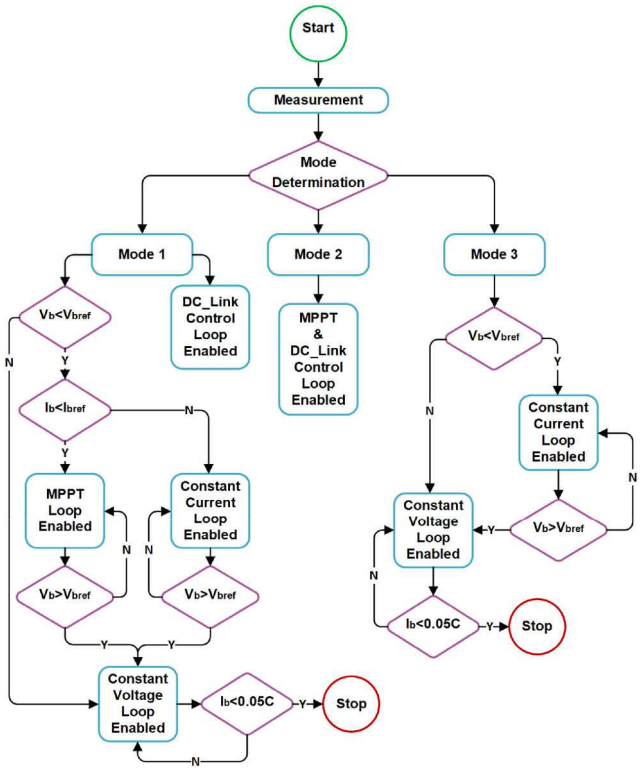

Fig. 9 *Overall control algorithm of the proposed system*

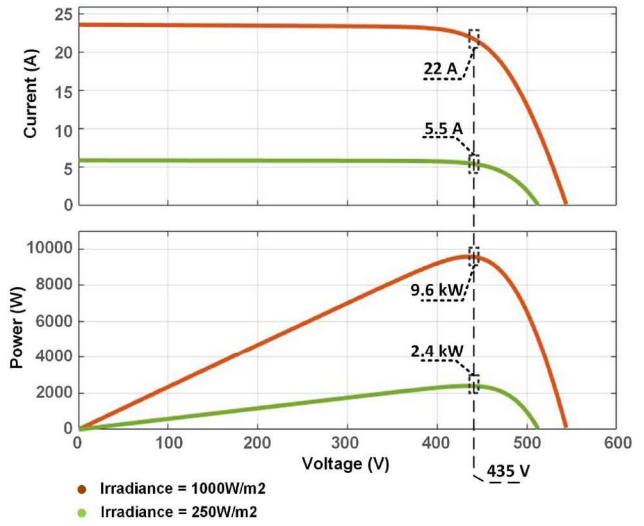

Fig. 10 *PV characteristics*

mode 2 by controlling the reference voltage of DC-link through the loops of DC-link control and P&O MPPT control. The DC-link controller adjusts the phase shift angle between the S_1 and S_4/S_2 and S_3. The reference value of the EM DC-link voltage (V_{dcref}) is subtracted from the measured DC-link voltage (V_{dc}) to calculate the error. The error signal is applied to the PI controller to generate the phase shift angle (ϕ). The overall control algorithm of the system is given in Fig. 9

$$\begin{cases} \text{CC charging} & V_{\text{b}} < V_{\text{bref}} \quad \text{and} \quad I_{\text{b}} \geq I_{\text{bref}} \\ I_{\text{b}} \text{ charging} & V_{\text{b}} < V_{\text{bref}} \quad \text{and} \quad I_{\text{b}} < I_{\text{bref}} \\ \text{CV charging} & V_{\text{b}} < V_{\text{bref}} \end{cases} \tag{12}$$

4 Performance analysis

This section presents the performance evaluation of the proposed system. To evaluate the performance of the qZ_iMPC topology and designed controllers, a standalone prototype is developed in a MATLAB/Simulink environment for 10 kVA EM fed by PV and ESU. The switching elements of power circuits are insulated-gate bipolar transistors because of the power rating and the switching frequency. In this study, a PV module in the rating of 9.6 kW, namely 1STH-215-P of the Soltech company, is used considering the actual irradiation parameter. The characteristic curves of PV under varying irradiance and constant temperature are illustrated in Fig. 10. The parameters of the developed system are shown in Table 1. The presented system is tested under two case studies summarised in Table 2. Case studies are formed in this way to verify that all modes can be performed by the proposed system.

Table 1 Parameters of the developed system

System	Parameter	Value
PV	PV maximum power (1000 W/m^2)	9.6 kW
	maximum power point voltage (1000 W/m^2)	435 V
	maximum power point current (1000 W/m^2)	22 A
	PV maximum power (250 W/m^2)	2.4 kW
	maximum power point voltage (250 W/m^2)	435 V
	maximum power point current (250 W/m^2)	5.5 A
	PV capacitor (C_{pv})	300 µF
ESU	battery capacity	60 Ah
	battery nominal voltage	200 V
	battery maximum charge current	30 A
	supercapacitor rated capacitance	1 F
	supercapacitor rated voltage	10 V
	supercapacitor number of series capacitor	4
	supercapacitor number of parallel capacitor	1
quasi-Z-source converter	quasi-Z-source inductors (L_{q1}, L_{q2})	1 mH
	quasi-Z-source capacitors (C_{q1}, C_{q2})	100 µF
general	DC-link capacitor (C_{out})	1000 µF
	nominal DC bus voltage	350 V
	switching frequency	20 kHz
	transformer turns ratio	1:1:1

Table 2 Details of case studies

	Case 1		Case 2	
	Time intervals		Time intervals	
	0–0.5 s	0.5–1 s	0–0.12 s	0.12–0.5 s
irradiation	1000 W/m^2	250 W/m^2	1000 W/m^2	250 W/m^2
temperature	25 C°	25 C°	25 C°	25 C°
EM demand	5 kW	5 kW	−3 kW	−3 kW
ESU charging/discharging	charging	discharging	charging (CC)	charging (CV)
mode transition	mode 1	mode 2	mode 3	mode 3

The first case corresponds to both mode 1 and mode 2, as well as dynamic responses in the transition between the two modes. The time interval of 0–0.5 s represents mode 1 with 1000 W/m^2 irradiation, 25 C° and 5 kW EM demand. Fig. 11 shows the steady-state and dynamic responses of the proposed system for case 1. The instantaneous PV power is higher than the power demand of the EM. Thus, the DC-link of the EM is controlled via PV through the DC-link controller. As illustrated in Fig. 11, the DC-link is kept under the desired voltage value and the power demand of the EM is provided. The difference between the EM demand and the instantaneous power of the PV corresponds to the charge power of ESU. It is clear that the instantaneous power values of the PV, ESU, and EM are 9.58, 4.2, and 5 kW, respectively. As shown in Fig. 11, the ESU is operated in charging mode and is charged with its nominal charge current since the available power of PV transferred to ESU is limited.

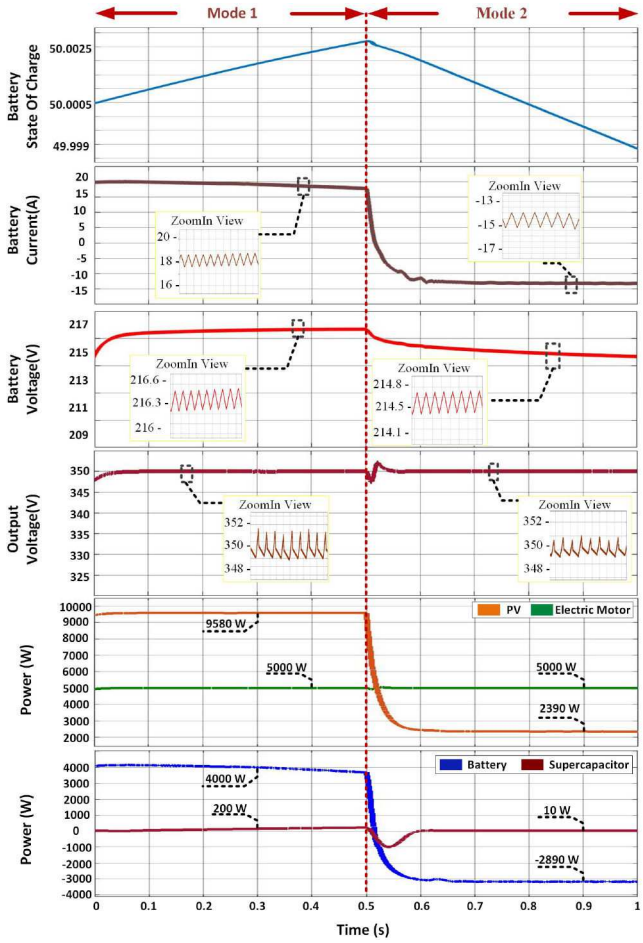

Fig. 11 *Results for case 1*

Table 3 Comparison of conventional converters and proposed qz_iMPC

Model	Port number	Number of switches	Efficiency, %	Bidirectional port
transformer coupled half-bridge [20]	3	6	91.5	ESU
transformer coupled full-bridge [17]	3	12	91	ESU
half-bridge [27]	3	4	94	ESU
full-bridge [28]	3	8	91	ESU
full-bridge interleaved [21]	4	8	96	ESU
proposed qz_iMPC	4	6	96	ESU, load

The dynamic performance of the standalone system is verified with the sudden change in the irradiation of the PV decreased to 250 from 1000 W/m^2. The time interval of 0.5–1 s represents mode 2 with 250 W/m^2 irradiation, 25 C° and 5 kW EM demand. During the current time interval, the PV generation power is not sufficient to supply the EM. The DC-link voltage cannot be kept constant via PV. As shown in Fig. 11, the power deficit is buffered by ESU and the DC-link is kept constant. It is clear that the instantaneous power values of the PV, ESU, and EM are 2.39, −2.88, and 5 kW, respectively. Thus, the ESU is operated in discharging mode. The supercapacitor discharges in milliseconds after the sudden change in the irradiation of the PV. In the current two time intervals, the P&O MPPT controller continuously tracks the maximum power point with the output voltage of 435 V and output current of 22 and 5.5 A, respectively.

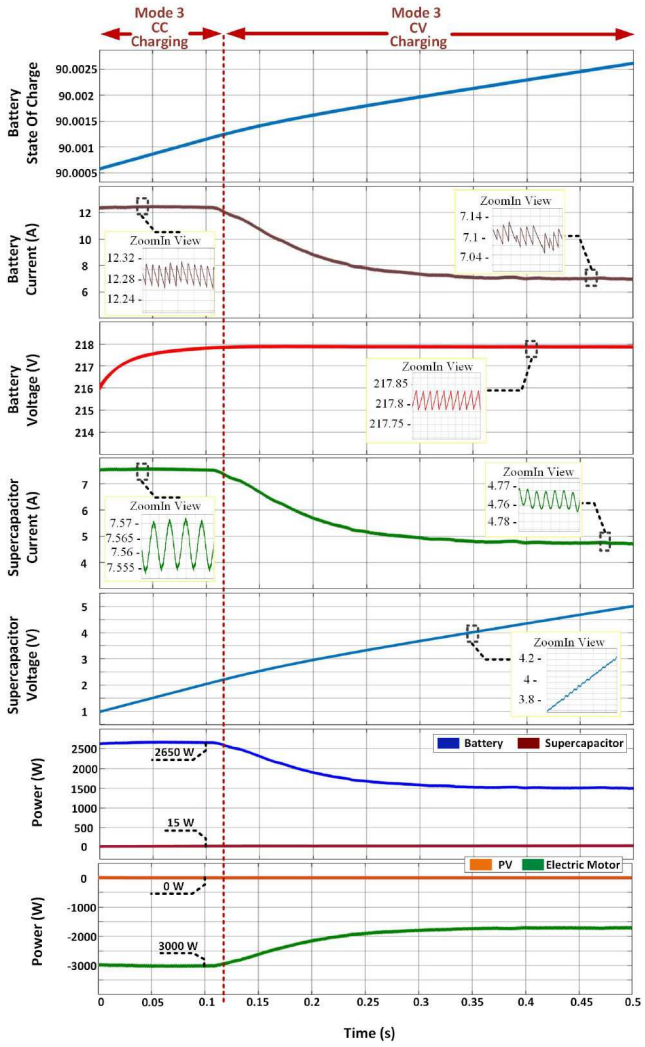

Fig. 12 *Results for case 2*

The second case corresponds mode 3. In the current mode, since it is not possible to transfer power to PV, the braking power is supplied to ESU. Fig. 12 shows the steady-state and dynamic responses of the proposed system for case 2. The time interval of 0–0.12 s represents the CC charging of the ESU unit for 3 kW braking power. As can be seen in Fig. 12, the charging current remains constant at its maximum allowable value until it switches to CV mode. It is clear that the charging current is 12.5 A. During the current time interval, the voltage of the ESU linearly increases with the braking power. When the battery voltage reaches the threshold value, the controller switches to the CV charging mode. The time interval of 0.12–0.5 s represents the CV charging of the ESU unit for 3 kW braking power. As illustrated in Fig. 12, the charging current decreases according to the state of the battery.

The efficiency analysis of the proposed system is performed for case 1, case 2, and case 3, considering the amount of generated electrical power of PV and absorbed/injected power of the EM. As can be seen from the power waveforms of PV, battery, supercapacitor, and EM in Figs. 11 and 12, the efficiency values of the proposed converter are 96.03, 94.87, and 88.83% for case 1, case 2, and case 3, respectively. The results reveal that the proposed system has high-efficiency values.

Table 3 outlines the comparative analysis between the proposed qz_iMPC and existing MPC topologies based on port number, number of switches, efficiency, and possible bidirectional power flow modes. Among these converters, the proposed converter excels with the advantages of reduced switch topology and high efficiency.

5 Conclusion

In this paper, a novel quasi-Z-source converter integrated isolated multiport bidirectional DC–DC converter topology and control method has been proposed. The main superior aspect of the proposed system is integrating four ports with reduced switch converter topology. Also, the proposed converter provides a high-voltage gain with a low amount of battery/supercapacitor voltages with less duty cycle. In addition, it allows designing a transformer with a low turn ratio, improving the efficiency of HFT. Thus, the voltage spikes caused by the leakage inductance of HFT are reduced. The functionalities of the proposed topology are: (i) providing uninterrupted power to the EM by PV and ESU, (ii) charging battery/supercapacitor packs via PV when the EM demand is lower than the PV power, (iii) charging battery/supercapacitor packs via the braking energy of the EM. The performance of the system is tested with different operational modes. As a result, the proposed system performs all power flow variations between the ports and implements all control methods which consist of CC/CV charging, MPPT, and DC-link control. The results and efficiency values for different cases validate the applicability of the proposed system.

6 References

[1] Ganjavi, A., Ghoreishy, H., Ahmad, A.A.: 'A novel single-input dual-output three-level DC–DC converter', *IEEE Trans. Ind. Electron.*, 2018, **65**, pp. 8101–8111

[2] Rashidi, M., Altin, N.N., Ozdemir, S.S., *et al.*: 'Design and development of a high-frequency multiport solid-state transformer with decoupled control scheme', *IEEE Trans. Ind. Appl.*, 2019, **55**, pp. 7515–7526

[3] Reddi, N.K., Ramteke, M.R., Suryawanshi, H.M., *et al.*: 'An isolated multi-input ZCS DC–DC front-end-converter based multilevel inverter for the integration of renewable energy sources', *IEEE Trans. Ind. Appl.*, 2018, **54**, pp. 494–504

[4] İnci, M., Türksoy, Ö.: 'Review of fuel cells to grid interface: configurations, technical challenges and trends', *J. Clean Prod.*, 2019, **213**, pp. 1353–1370

[5] Zhang, N., Sutanto, D., Muttaqi, K.M.: 'A review of topologies of three-port DC–DC converters for the integration of renewable energy and energy storage system', *Renew. Sustain. Energy Rev.*, 2016, **56**, pp. 388–401

[6] Bhattacharjee, A.K., Kutkut, N., Batarseh, I.: 'Review of multiport converters for solar and energy storage integration', *IEEE Trans. Power Electron.*, 2019, **34**, pp. 1431–1445

[7] Khosrogorji, S., Ahmadian, M., Torkaman, H., *et al.*: 'Multi-input DC/DC converters in connection with distributed generation units – a review', *Renew. Sustain. Energy Rev.*, 2016, **66**, pp. 360–379

[8] Akar, F., Tavlasoglu, Y., Vural, B.: 'An energy management strategy for a concept battery/ultracapacitor electric vehicle with improved battery life', *IEEE Trans. Transp. Electrification*, 2017, **3**, pp. 191–200

[9] Hu, S., Liang, Z., Fan, D., *et al.*: 'Hybrid ultracapacitor–battery energy storage system based on quasi-Z-source topology and enhanced frequency dividing coordinated control for EV', *IEEE Trans. Power Electron.*, 2016, **31**, pp. 7598–7610

[10] Shen, J., Khaligh, A.: 'A supervisory energy management control strategy in a battery/ultracapacitor hybrid energy storage system', *IEEE Trans. Transp. Electrification*, 2015, **1**, pp. 223–231

[11] Hu, S., Liang, Z., He, X.: 'Ultracapacitor-battery hybrid energy storage system based on the asymmetric bidirectional Z-source topology for EV', *IEEE Trans. Power Electron.*, 2016, **31**, pp. 7489–7498

[12] Lu, J., Wang, Y., Li, X., *et al.*: 'High-conversion-ratio isolated bidirectional DC–DC converter for distributed energy storage systems', *IEEE Trans. Power Electron.*, 2019, **34**, pp. 7256–7277

[13] Akagi, H., Kinouchi, S., Miyazaki, Y.: 'Bidirectional isolated dual-active-bridge (DAB) DC–DC converters using 1.2-kV 400-A SiC-MOSFET dual modules', *CPSS Trans. Power Electron. Appl.*, 2016, **1**, pp. 33–40

[14] Savrun, M.M., Köroğlu, T., Tan, A., *et al.*: 'Isolated H-bridge DC–DC converter integrated transformerless DVR for power quality improvement', *IET Power Electron.*, 2020, **13**, pp. 920–926

[15] Hou, N., Song, W., Wu, M.: 'Minimum-current-stress scheme of dual active bridge DC–DC converter with unified phase-shift control', *IEEE Trans. Power Electron.*, 2016, **31**, pp. 8552–8561

[16] Farhangi, B., Toliyat, H.A.: 'Modeling and analyzing multiport isolation transformer capacitive components for onboard vehicular power conditioners', *IEEE Trans. Ind. Electron.*, 2015, **62**, pp. 3134–3142

[17] Phattanasak, M., Gavagsaz-Ghoachani, R., Martin, J., *et al.*: 'Control of a hybrid energy source comprising a fuel cell and two storage devices using isolated three-port bidirectional DC–DC converters', *IEEE Trans. Ind. Appl.*, 2015, **51**, pp. 491–497

[18] Karanayil, B., Ciobotaru, M., Agelidis, V.G.: 'Power flow management of isolated multiport converter for more electric aircraft', *IEEE Trans. Power Electron.*, 2017, **32**, pp. 5850–5861

[19] Wang, Y., Han, F., Yang, L., *et al.*: 'A three-port bidirectional multi-element resonant converter with decoupled power flow management for hybrid energy storage systems', *IEEE Access*, 2018, **6**, pp. 61331–61341

[20] Wang, L., Wang, Z., Li, H.: 'Asymmetrical duty cycle control and decoupled power flow design of a three-port bidirectional DC–DC converter for fuel cell vehicle application', *IEEE Trans. Power Electron.*, 2012, **27**, pp. 891–904

[21] Wu, H., Zhang, J., Qin, X., *et al.*: 'Secondary-side-regulated soft-switching full-bridge three-port converter based on bridgeless boost rectifier and bidirectional converter for multiple energy interface', *IEEE Trans. Power Electron.*, 2016, **31**, pp. 4847–4860

[22] Ding, Z., Yang, C., Zhang, Z., *et al.*: 'A novel soft-switching multiport bidirectional DC–DC converter for hybrid energy storage system', *IEEE Trans. Power Electron.*, 2014, **29**, pp. 1595–1609

[23] Jakka, V.N.S.R., Shukla, A., Demetriades, G.D.: 'Dual-transformer-based asymmetrical triple-port active bridge (DT-ATAB) isolated DC–DC converter', *IEEE Trans. Ind. Electron.*, 2017, **64**, pp. 4549–4560

[24] Li, W., Xiao, J., Zhao, Y., *et al.*: 'PWM plus phase angle shift (PPAS) control scheme for combined multiport DC/DC converters', *IEEE Trans. Power Electron.*, 2012, **27**, pp. 1479–1489

[25] Hong, J., Yin, J., Liu, Y., *et al.*: 'Energy management and control strategy of photovoltaic/battery hybrid distributed power generation systems with an integrated three-port power converter', *IEEE Access*, 2019, **7**, pp. 82838–82847

[26] Wu, H., Chen, R., Zhang, J., *et al.*: 'A family of three-port half-bridge converters for a stand-alone renewable power system', *IEEE Trans. Power Electron.*, 2011, **26**, pp. 2697–2706

[27] Zhu, H., Zhang, D., Athab, H.S., *et al.*: 'PV isolated three-port converter and energy-balancing control method for PV-battery power supply applications', *IEEE Trans. Ind. Electron.*, 2015, **62**, pp. 3595–3606

[28] Itoh, K., Ishigaki, M., Yanagizawa, N., *et al.*: 'Analysis and design of a multiport converter using a magnetic coupling inductor technique', *IEEE Trans. Ind. Appl.*, 2015, **51**, pp. 1713–1721

[29] Lee, I., Moon, G.: 'Analysis and design of phase-shifted dual H-bridge converter with a wide ZVS range and reduced output filter', *IEEE Trans. Ind. Electron.*, 2013, **60**, pp. 4415–4426

[30] Ahmed, N.A., Madouh, J.Y.: 'High-frequency full-bridge isolated DC–DC converter for fuel cell power generation systems', *Electr. Eng.*, 2018, **100**, pp. 239–251

[31] Liu, Y., Abu-Rub, H., Ge, B., *et al.*: 'Voltage-Fed Z-Source/Quasi-Z-Source Inverters', in Liu, Y., Abu-Rub, H., Ge, B. (Eds.): *Impedance Source Power Electronic Converters* (Wiley-IEEE Press, UK, 2016), pp. 20–34

[32] Khajesalehi, J., Hamzeh, M., Sheshyekani, K., *et al.*: 'Modeling and control of quasi Z-source inverters for parallel operation of battery energy storage systems: application to microgrids', *Electr. Power Syst. Res.*, 2015, **125**, pp. 164–173